Search for Anomalous Diphoton Plus X Production

The CDF Collaboration
URL http://www-cdf.fnal.gov
(Dated: August 9, 2007)

This note describes a search for events with two photons and additional identified objects. So far, the additional object may be $\not\!\!E_t$, an electron, a muon, or a third photon. The data were collected in $\bar{p}p$ collisions at $\sqrt{s} = 1.96$ TeV with the CDF detector at the Fermilab Tevatron, Run II. We use nominal high-E_T object identification and kinematic selections. We report observed event counts, Standard Model background predictions, and kinematic distributions.

I. INTRODUCTION

Some models of new physics that predict two photons in the final state include Gauge–mediated SUSY, fermiphobic Higgs, $\chi_2^0 \to \gamma\chi_1^0$, b' pairs, and production of a pair of excited particles which decay to $\gamma + X$. With the large range of exotics models, both known and not yet imagined, and vanishing odds of selecting the correct model, we chose to perform searches based on the final state signature. This work significantly extends previous CDF diphoton searches [1]. The next section describes the diphoton event selection and the following sections describe the search for each X.

The data were collected between February 2002 and February 2006. Since each final state may require different parts of the detector to be operating for proper identification, the integrated luminosity is different for different final states, and is reported below. The CDF detector is described in detail in [2].

II. DIPHOTON DATA SAMPLE AND EVENT SELECTION

Diphoton events are collected by two triggers, the first has an E_T threshold of 12 GeV and requires the electromagnetic shower to be isolated in the calorimeter. A second trigger with an E_T threshold of 18 GeV has no isolation requirement. We accept event selected by either of the triggers.

The diphoton sample is selected offline by requiring two central ($|\eta| < 1$) electromagnetic showers. The shower shape in the shower maximum detector must be consistent with a single shower. The cluster must be isolated in the calorimeter ($E_T < 2$ GeV in a cone of 0.4 in $\eta - \phi$ space), in the tracking system ($E_T < 2$ GeV in a cone of 0.4) and in the shower maximum detector. We require that both photons pass the cuts, and have $E_T > 13$ GeV. We require the events have a vertex with $|z| < 60$ cm.

III. DIPHOTON PLUS $\not\!\!E_T$

In this part of the analysis, we search for anomalous production of $\gamma\gamma$ pairs in association with significant $\not\!\!E_t$ in 1.156 fb^{-1} of data. Events selected by di-photon triggers (see Section II) are split into two samples: $\gamma\gamma$ signal and control samples. Photons from the signal sample are required to pass a standard set of photon ID cuts (see Section II). The control sample is formed by events where both photons pass loose photon ID cuts and at least one photon fails the standard cuts. The loose ID cuts differ from the standard ones by relaxed requirements on photon isolation in the calorimeter (E_T <3 GeV in cone of 0.4), tracking system (E_T <5 GeV in cone of 0.4) and shower maximum detector (no requirement). Events from signal and control samples are required to have a vertex with $|z|$ <60 cm. If there is more than one vertex per event, all vertices must have $|z|$ <60 cm, and the maximum separation between the highest $\sum P_T^{trk}$ (best) vertex and any other vertex is required to be less than 90 cm. In order to suppress background due to cosmic rays, both photon candidates (in $\gamma\gamma$ signal and control samples) must have time of arrival (as measured by EM timing system [3]) consistent with the time of a hard collision. In runs when timing information is not available, we reject events if there are trackless muon stubs in cones of 30^o around a direction of any photon. Events where one or both photon candidates are consistent with a signature produced by beam halo muons are also rejected. All events are examined for evidence of spurious energy due to photo-tube spikes. (Only 2 events in signal and 3 events in control samples have such signatures and have been rejected.) Finally, we apply $\not\!\!E_t$ clean up cuts to remove events where $\not\!\!E_t$ is along the jet direction ($\Delta\phi = \phi_{\not E_t} - \phi_{jet}$ <0.1 rad) and this jet points to poorly instrumented region of the calorimeter. After all of the selection cuts, we have 18,230 and 27,871 events in the signal and control samples, respectively.

The $\gamma\gamma$ signal and control samples contain ~30% and ~5% of real $\gamma\gamma$ events, respectively [1]. Most of the remaining events are either $\gamma + jet \to \gamma\gamma_{fake}$ or $jet + jet \to \gamma_{fake}\gamma_{fake}$, where γ_{fake} are photons from decays of energetic π^0, η or K_s^0 in jets. The $\gamma\gamma$ control sample is used to develop and check performance of the background evaluation techniques, because it has three important qualities: *1)* small fraction of real $\gamma\gamma$ events; *2)* same topology and similar kinematic properties as the $\gamma\gamma$ signal sample; *3)* same sources of $\not\!\!E_t$ backgrounds as in the signal sample. The $\not\!\!E_t$ in $\gamma\gamma$ events is corrected for the vertex position and for the difference between raw and corrected energy of all jets with E_T^{corr} >15 GeV. In events with 2 or more vertices, we calculate $\not\!\!E_t$ with respect to the vertex that minimizes it.

There are three major sources of background for $\gamma\gamma + \not\!\!E_t$ signature in the final state:

- Inclusive $e\gamma$ events with real intrinsic $\not\!\!E_t$:
  The $\gamma\gamma$ events where one of the photon candidates is really an electron which lost its track either due to tracking inefficiency or, more often, collinear FSR and hard bremsstrahlung in the detector material in front of the tracker. Many Standard Model processes with electrons in the final state have intrinsic $\not\!\!E_t$ (e.g., inclusive $W \to e\bar{\nu}$ production, $b \to e\bar{\nu}X$, or $\tau \to e\bar{\nu}_e\nu_\tau X$). The contribution due to this source of background is evaluated

$\not{E}_t$-cut, GeV	Background	Data
$\not{E}_t \geq 20$	115.9±3.2±23.4	126
$\not{E}_t \geq 25$	38.3±1.7±6.5	42
$\not{E}_t \geq 30$	19.5±1.1±2.3	22
$\not{E}_t \geq 35$	10.8±0.7±1.4	15
$\not{E}_t \geq 40$	4.2±0.4±0.8	9
$\not{E}_t \geq 45$	2.1±0.3±0.3	6
$\not{E}_t \geq 50$	1.6±0.3±0.2	4
$\not{E}_t \geq 75$	0.24±0.08±0.21	1
$\not{E}_t \geq 100$	0.048±0.025±0.036	1
$\not{E}_t \geq 150$	0.024±0.013±0.022	1

TABLE I: Summary of results in $\gamma\gamma + \not{E}_t$ signal region.

based on the $\not{E}_t$ distribution in $e\gamma$ events scaled by the E_T-dependent probability of an electron faking photon. This probability is $\sim$0.70±0.08% at $E_T \sim$40 GeV.

- Non-collision events:
  Events where muons from cosmic rays or beam halo are faking one or more photons and $\not{E}_t$. The contribution due to cosmic rays is evaluated based on the $\not{E}_t$ distribution in out-of-time $\gamma\gamma$-like events passing all of the cuts and a known rate of such cosmic events arriving in time with the hard collision. The contribution due to beam halo events is estimated based on the $\not{E}_t$ distribution in observed beam halo events and a known efficiency and mis-identification rate of the beam halo rejection cuts.

- QCD events with fake $\not{E}_t$:
  True $\gamma\gamma$, $\gamma - jet \rightarrow \gamma\gamma_{fake}$, and $jet - jet \rightarrow \gamma_{fake}\gamma_{fake}$ events where $\not{E}_t$ arises due to energy mis-measurement in the calorimeter. We predict the shape of fake $\not{E}_t$ by means of the *Met Resolution Model* parametrized in terms of the observed soft energy (all energy except for energy of identified photons and jets) and energy of all jets in a given event. The *Met Resolution Model* is based on the assumption that individual particle's energy resolution has Gaussian shape and it is proportional to particle's $\sqrt{E_T}$. To simplify the model, we distinguish only two sources of fake $\not{E}_t$: soft unclustered energy (underlying event, multiple interactions), and jets. The unclustered energy tends to be uniformly spread in the calorimeter. Therefore, the portion of $\not{E}_t$ due to this source is usually small. Jets, unlike soft energy, are collimated sprays of energetic particles in a certain direction and, because of this nature, they tend to produce most of $\not{E}_t$. To obtain $\not{E}_t$ resolution due to the unclustered energy, we study the $\gamma\gamma$ control and $Z \rightarrow e^+e^-$ samples with no jets with E_T^{corr} >15 GeV. We use a known jet energy resolution ($\sim$25% at $E_T \sim$20 GeV), to predict the jet's contribution to $\not{E}_t$. For each $\gamma\gamma$ event, we randomly generate the expected $\not{E}_t$ contribution due to the unclustered component of energy deposited in the calorimeter. Then, we take all jets with $E_T^{corr} > 3$ GeV in the event and smear their energies according to the known resolution. If the jet's smeared energy, E_T^{smear}, is above 15 GeV threshold, we calculate that jet's contribution into $\not{E}_t$: $\vec{\not{E}}_t^{jet,i} = \vec{E}_T^{corr} - \vec{E}_T^{smear}$. Finally, we sum up all of the individual $\not{E}_t$ components due to the soft unclustered energy and each of the jets with $E_T^{smear} > 15$ GeV to obtain our final prediction.

The background predictions are obtained for various thresholds of $\not{E}_t$-cut and compared to corresponding numbers of observed events in signal and control samples. The results of this comparison can be found in Tables I and II. The $\not{E}_t$ distribution in $\gamma\gamma$ events signal and control samples are shown on Figs. 1 and 2, respectively. We also study $M_{\gamma\gamma}$, H_T and $N_{jet}(E_T{>}15)$ distributions in signal and control sample events with $\not{E}_t$>20 GeV (see Figs. 3-5). No significant discrepancy between data and background predictions is observed in either of the distributions.

IV. DIPHOTON PLUS ELECTRON OR MUON

In this part of the analysis, we search for an excess with respect to Standard Model prediction in the events with two central photons ($|\eta| < 1$) and additional electron ($|\eta| < 2.0$) or central muon ($|\eta| < 1.0$). Data used for this analysis comprise an integrated luminosity of 1020–1100 pb^{-1} and were collected with the diphoton trigger. The tracking system, central and forward calorimeters, and central muon chamber are required to be working properly. The central photon candidates with $E_T > 13$ GeV each, electron candidates with $E_T > 20$ GeV and muon candidates with $P_T > 20$ GeV/c, are then required to satisfy the same criteria as those in [1, 4]. After the event selection, we observe three $\gamma\gamma e$ events and zero $\gamma\gamma\mu$ event. We further remove events with photons matched to the electron tracks

$\not\!\!E_t$-cut, GeV	Background	Data
$\not\!\!E_t \geq 20$	174.0±4.4±34.1	196
$\not\!\!E_t \geq 25$	58.4±2.7±10.2	68
$\not\!\!E_t \geq 30$	26.2±2.0±4.1	31
$\not\!\!E_t \geq 35$	13.6±1.5±2.1	13
$\not\!\!E_t \geq 40$	6.7±1.0±0.8	4
$\not\!\!E_t \geq 45$	3.9±0.7±0.5	3
$\not\!\!E_t \geq 50$	2.5±0.7±0.3	2
$\not\!\!E_t \geq 75$	0.89±0.45±0.14	0
$\not\!\!E_t \geq 100$	0.40±0.35±0.08	0
$\not\!\!E_t \geq 150$	0.025±0.014±0.027	0

TABLE II: Summary of results in $\gamma\gamma + \not\!\!E_t$ control region.

reconstructed in the silicon detector seeded by the cluster in the electromagnetic calorimeter (Phoenix rejection). The observed number of $\gamma\gamma e$ events is reduced to one. These removed photons come from the electrons bremsstrahlung outside of the silicon tracking volume. The observed number of events in data are to be compared with the Standard Model prediction described below.

Several processes could produce the signature of "$\gamma\gamma e$ or $\gamma\gamma\mu$". In order to avoid double-counting, they are grouped into the following categories:

1. true photons and true lepton from the Standard Model $Z\gamma\gamma$ and $W\gamma\gamma$ tri-boson production
2. fake photons or leptons
    - true photons and fake lepton
    - fake photons from jets
    - fake photons from electrons with a lost track
    - fake photons from cosmic rays

The Standard Model production of $Z\gamma\gamma$ and $W\gamma\gamma$ is estimated with the Monte Carlo (MC). The MC sample is generated using a leading-order (LO) matrix element generator `Madgraph` [5]. The output of `Madgraph` is fed into `PYTHIA` [6] to add parton fragmentation, initial- and final-state QCD and QED radiation. The output of `PYTHIA` is then run through a full CDF detector simulation and the same analysis program as that for the data. Proper data/MC efficiency scale factors are applied. In addition, the `Madgraph` LO cross-sections are scaled to the next-to-leading-order (NLO) cross-sections according to the K-factors derived in [7].

The number of "true $\gamma\gamma$ + fake lepton" events is extracted in the following way: First, the number of "diphoton candidate + fake lepton" events is obtained by applying an E_T-dependent fake probability from [8] to the events with a diphoton candidate and an object which may fake a lepton. These fakeable objects are jets for electrons and isolated tracks for muons. The fake probability has an average of about 0.04% for electrons, and 1.0% for muons, with a 50% systematic uncertainty each. Second, the observed diphoton candidates could also be fakes. In order to avoid overlapping with the fake photon estimate described below, the number of "diphoton candidate + fake lepton" events is multiplied with the true $\gamma\gamma$ fraction in the diphoton sample, which gives the number of "true $\gamma\gamma$ + fake lepton" events. The true $\gamma\gamma$ fraction was estimated to be (29±4)% for $E_T(\gamma) > 13$ GeV in [1].

Fake photons arise from jets containing π^0, η or K_s^0, a hard bremsstrahlung of electrons, or cosmic rays. Although these sources give real photons in the final state, they are considered fakes in this analysis, to be distinguished from the photons produced by the ISR, FSR or the hard scattering process. Numbers of fake photons from jets and electrons are estimated by applying the E_T-dependent fake probability to the events with a lepton candidate, a photon candidate and a fakeable object (jets or electrons). The jet faking photon rate [7] is about 0.2% at $E_T(\gamma)$ =13 GeV and 0.04% for $E_T(\gamma)$ >50 GeV, with a systematic uncertainty ranging from 50% to 200%. The average electron faking photon rate is about 1.5% and 0.4% before and after applying the Phoenix rejection, with an 11% and 17% systematic uncertainty, respectively. Finally, the probability for a photon event to overlap with a cosmic event was found to be about $1.5{\cdot}10^{-8}$ in [1]. Therefore, the number of fake photons from the cosmic rays is estimated by applying this probability to events with a lepton candidate and a photon candidate. There is less than 10^{-5} and 10^{-6} cosmic events for the electron and muon channels, respectively. In addition, timings of the photon and electron candidates in the observed $\gamma\gamma + e$ events, reported by the CDF II Timing System for the Electromagnetic Calorimeters (EM TDC) [3], are within the RMS of the beam collision time and the intrinsic resolution of EM TDC and are considered "prompt" events.

TABLE III: Summary of the predicted number of $\gamma\gamma e$ or $\gamma\gamma\mu$ events and that of observed events in the 1020–1100 pb^{-1} of data, for $E_T(\gamma) > 13$ GeV. The first uncertainty of each background category is statistical. The second uncertainty is the systematic uncertainty either from the data luminosity, LO cross-section and K-factor, or from the fake rates. The statistical and systematic uncertainties are combined into one in the total number of predicted events.

Before applying Phoenix rejection		
Source	electron	muon
$Z\gamma\gamma$	0.904 ± 0.023 ± 0.083	0.552 ± 0.017 ± 0.050
$W\gamma\gamma$	0.170 ± 0.012 ± 0.016	0.086 ± 0.008 ± 0.008
Fake l+$\gamma\gamma$	0.131 ± 0.004 ± 0.053	0.004 ± 0.003 ± 0.002
$l\gamma+\text{jet}\to\gamma$	0.475 ± 0.025 ± 0.312	0.133 ± 0.013 ± 0.090
$l\gamma+e\to\gamma$	5.140 ± 0.340 ± 0.584	0.017 ± 0.017 ± 0.002
Total	6.82 ± 0.75	0.79 ± 0.11
Data	3	0

After applying Phoenix rejection		
Source	electron	muon
$Z\gamma\gamma$	0.816 ± 0.021 ± 0.074	0.498 ± 0.016 ± 0.045
$W\gamma\gamma$	0.153 ± 0.011 ± 0.014	0.078 ± 0.008 ± 0.007
Fake l+$\gamma\gamma$	0.118 ± 0.004 ± 0.049	0.004 ± 0.003 ± 0.002
$l\gamma+\text{jet}\to\gamma$	0.439 ± 0.023 ± 0.263	0.123 ± 0.012 ± 0.083
$l\gamma+e\to\gamma$	2.261 ± 0.211 ± 0.411	0.004 ± 0.004 ± 0.001
Total	3.79 ± 0.54	0.71 ± 0.10
Data	1	0

Table III summarizes the number of $\gamma\gamma e$ or $\gamma\gamma\mu$ events for photons E_T greater than 13 GeV from the prediction and that observed in data. The overall p-values given the numbers of observed and predicted events are both larger than 40% before and after the Phoenix rejection. The leading background in the electron channel is fake photons from electrons. The leading background in the muon channel is the electroweak tri-boson production of $Z\gamma\gamma$. Figures 6–7 show several important kinematic distributions from the predicted events overlayed with those observed in the data, before applying Phoenix rejection. We also repeat the same analysis procedure with looser photon identification requirements. The deficit of $\gamma\gamma e$ events in data, both with standard and loose photon requirements, has prompted a thorough study of backgrounds in the electron channel. We have cross-check our background estimate using independent methods and obtained consistent results with the prediction described earlier. We believe the deficit is a downward statistical fluctuation.

V. DIPHOTON PLUS THIRD PHOTON

The integrated luminosity for this search is 1155 pb^{-1}. The third photon must be central and must pass the same requirements as the first two photons. We find 21452 diphoton events and 4 triphoton events. The events have been examined for evidence that any clusters are caused by cosmic rays, phototube spikes or other pathologies. All events pass checks and estimated backgrounds from these sources are negligible.

There are two known Standard Model contributions to this sample. The first is true triphoton production. We estimate this source from `Madgraph` [5] Monte Carlo and apply an estimated k-factor of 1.5 ± 0.2 [9]. The second source is when at least one of the photons is a jet that has faked a photon, primarily by fragmenting to a leading π^0. We estimate these events by counting the jets in the diphoton sample, and multiplying by a E_T–dependent probability for a jet to fake an isolated photon. These probabilities are on the order of 4×10^{-4} for E_T >25 GeV.

The resulting Standard Model estimate is shown in Table IV. Kinematic distributions are shown in Figures 8 through 12.

VI. DIPHOTON PLUS TAU

The integrated luminosity for this search is 2014 pb^{-1}.

We identify taus in two stages, starting with a loose selection:

Source	Number
triphoton	0.8 ± 0.15
fakes	1.4 ± 0.6
total	2.2 ± 0.6
observed	4

TABLE IV: The estimated backgrounds to the Triphoton search. The uncertainties are systematic.

- well-measured seed track with $P_T > 4.5$ GeV
- seed track fiducial to central shower max detector
- electron rejection using EM fraction

the final tau selection then also includes:

- visible mass < 1.8 GeV/c^2
- track isolation in an E_T-dependent isolation cone < 1.0 GeV
- reconstructed π^0 in an E_T-dependent isolation cone < 0.6 GeV
- 1 or 3 tracks in $10°$ cone
- total track charge ± 1

The largest background to taus is jets which accidentally pass tau cuts (fake taus). To estimate this background we will derive a tau fake rate, and apply it to a denominator sample consisting of diphtons and a loose tau. The fake rate then is the probability for a loose tau from a jet to pass tight tau cuts. The probability is measured in the inclusive jet trigger samples, and is displayed in 13.

To test the fake rate, we create three control samples: events with two loose photons, events with one central and one plug photon, and events with a loose central photon and a plug photon. The result of applying the tau fake rate to these samples, compared to the observed tau yield, is shown in Table V.

Sideband sample check	
Source	Number
fakes	59 ± 14
observed	62
CP sample check	
Source	Number
fakes	63 ± 15
observed	67
CP Sideband sample check	
Source	Number
fakes	184 ± 44
observed	193

TABLE V: The results of applying the tau fake rate to control samples.

As part of the fake rate study, we find that jets originating from a quark are three times more likely to fake a tau than jets which originate from a gluon. We also find the fraction of jets which originate from quarks is different between the inclusive jet sample and the diphoton sample, according to our PYTHIA [6] Monte Carlo generator. These two facts imply we should derive a correction to the fake prediction which allows for quark fraction. This correction multiplies the fake prediction by 1.21.

We estimate a 20% systematic uncertainty for the tau fake rate, from its ability to predict distributions in control samples. We estimate a 13% systematic uncertainty in the quark fraction correction, from varying the way the quarks and gluons are counted.

In the fakes study, we predict background for real and fake photons, but always with a fake tau. We then add an estimate of background from real taus using MadGraph $W\gamma$ amd $Z\gamma$ samples. The backgrounds are summarized in Table VI.

The resulting total Standard Model estimate is shown in Table VI. Kinematic distributions are shown in Figures 14 through 18.

Source	Number
fakes	44 ± 10
$W\gamma$	1.2 ± 0.7
$Z\gamma$	1.0 ± 0.3
total	46 ± 10
observed	34

TABLE VI: The estimated backgrounds to the Diphoton and tau search. The uncertainties are systematic.

Acknowledgments

We thank the Fermilab staff and the technical staffs of the participating institutions for their vital contributions. This work was supported by the U.S. Department of Energy and National Science Foundation; the Italian Istituto Nazionale di Fisica Nucleare; the Ministry of Education, Culture, Sports, Science and Technology of Japan; the Natural Sciences and Engineering Research Council of Canada; the National Science Council of the Republic of China; the Swiss National Science Foundation; the A.P. Sloan Foundation; the Bundesministerium fuer Bildung und Forschung, Germany; the Korean Science and Engineering Foundation and the Korean Research Foundation; the Particle Physics and Astronomy Research Council and the Royal Society, UK; the Russian Foundation for Basic Research; the Comision Interministerial de Ciencia y Tecnologia, Spain; and in part by the European Community's Human Potential Programme under contract HPRN-CT-20002, Probe for New Physics.

[1] D. Acosta, et al., Phys. Rev. D **71**, 031104 (2005); F. Abe, et al., Phys. Rev. Lett., **81** 1791 (1998); F. Abe, et al., Phys. Rev. D **59**, 092002 (1999).
[2] F. Abe, et al., Nucl. Instrum. Methods Phys. Res. A **271**, 387 (1988); D. Amidei, et al., Nucl. Instum. Methods Phys. Res. A **350**, 73 (1994); F. Abe, et al., Phys. Rev. D **52**, 4784 (1995); P. Azzi, et al., Nucl. Instrum. Methods Phys. Res. A **360**, 137 (1995); The CDFII Detector Technical Design Report, Fermilab-Pub-96/390-E
[3] M. Goncharov *et al.*, arXiv:physics/0512171.
[4] D. Acosta *et al.* [CDF Collaboration], Phys. Rev. D **72**, 052003 (2005)
[5] F. Maltoni and T. Stelzer, "Madgraph", Comput. Phys. Commum. **357**, 81 (1994)
[6] T. Sjostrand et al., High-Energy-Physics Event Generation with PYTHIA 6.1, Comput. Phys. Commun. **135**, 238 (2001).
[7] D. Acosta *et al.* [CDF II Collaboration], Phys. Rev. Lett. **94**, 041803 (2005)
[8] A. Canepa *et al.* [CDF II Collaboration], FERMILAB-CONF-05-595-E
[9] Jean-Phillipe Guillet, private communication.

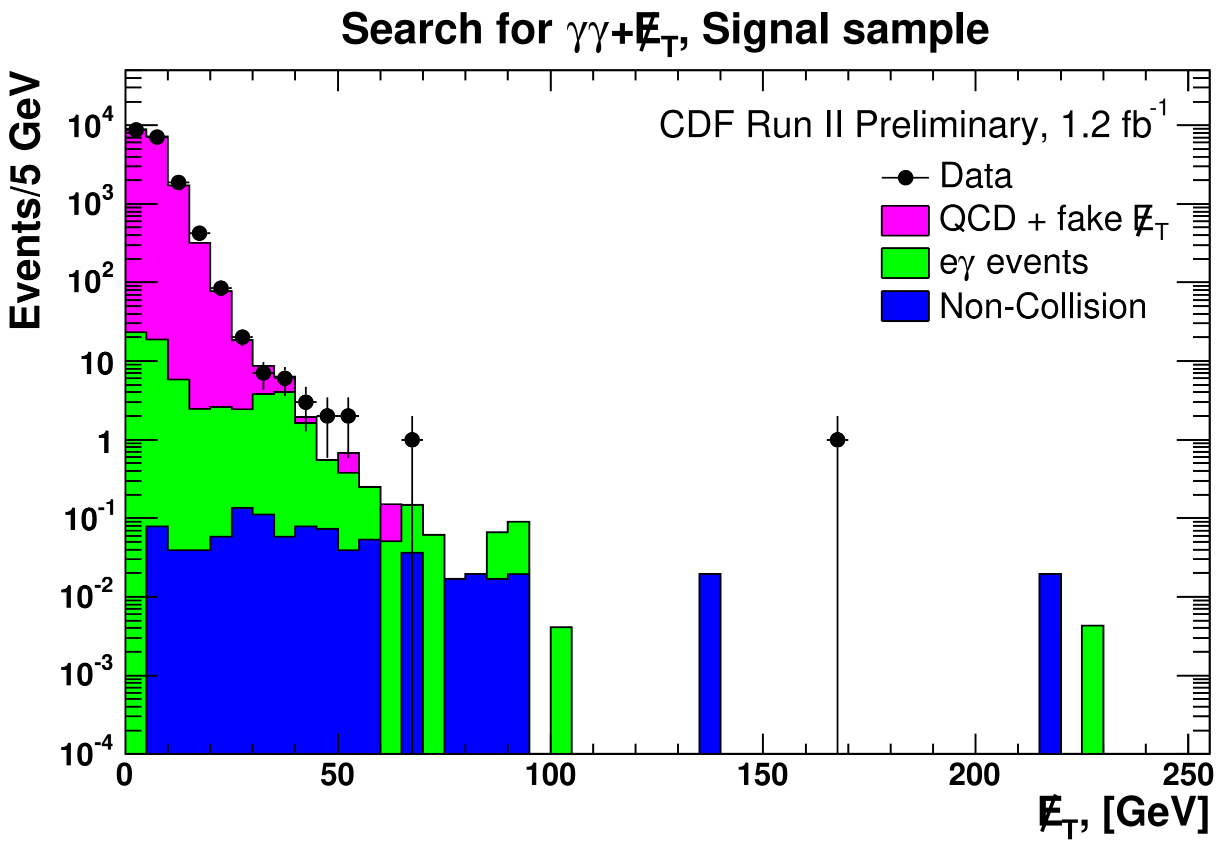

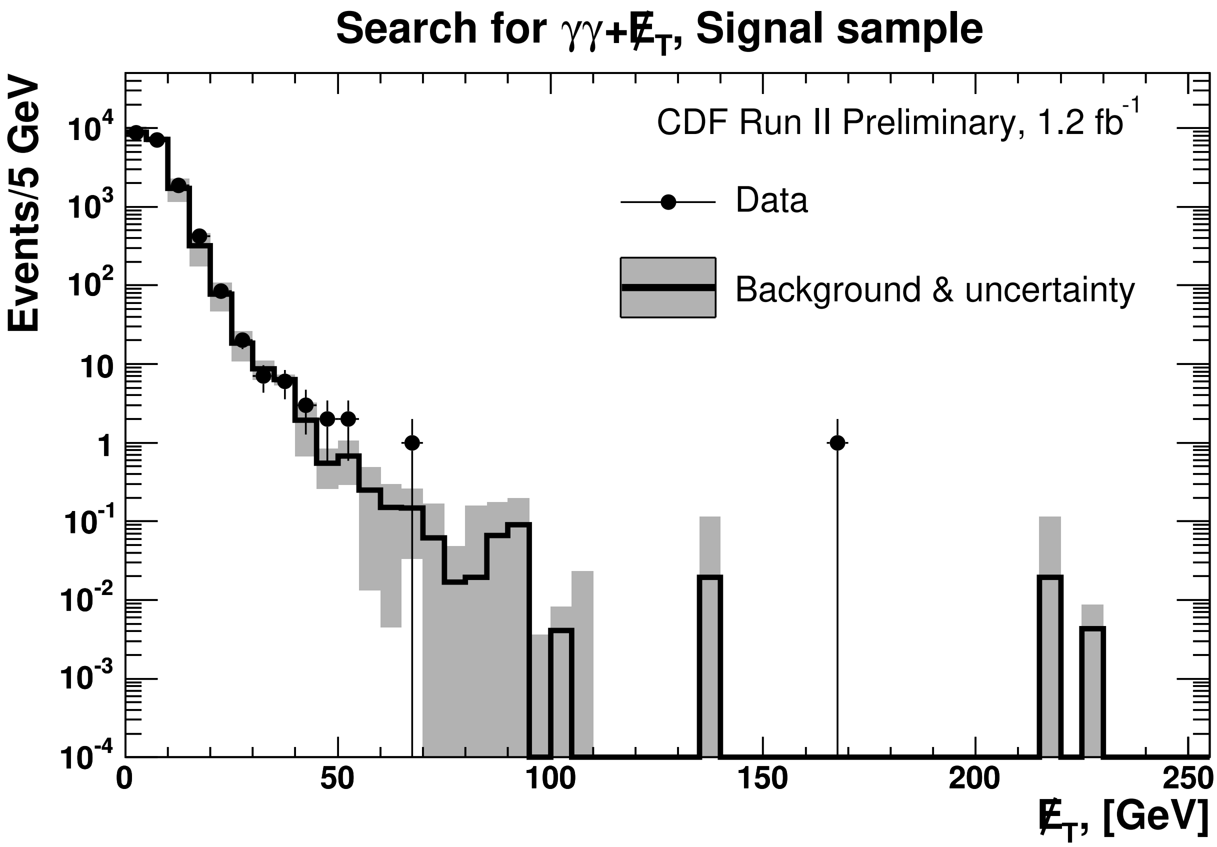

FIG. 1: The $\not{E}_t$ distribution and background predictions for $\gamma\gamma$ events from the signal sample. The upper plot shows the background composition. The lower plot shows data compared to the total background (solid line) with uncertainties (gray band).

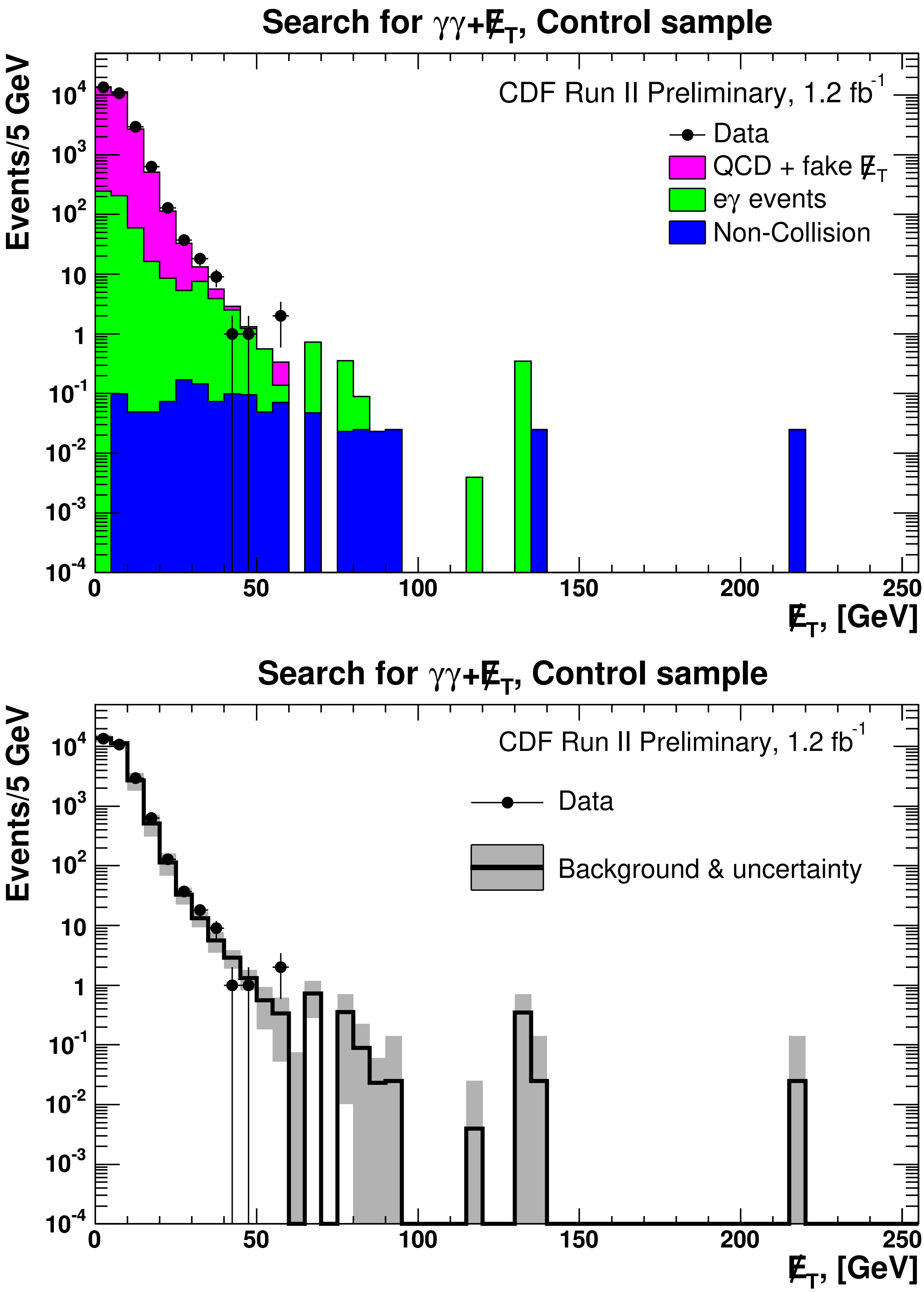

FIG. 2: The $\not\!E_t$ distribution and background predictions for $\gamma\gamma$ events from the control sample. The upper plot shows the background composition. The lower plot shows data compared to the total background (solid line) with uncertainties (gray band).

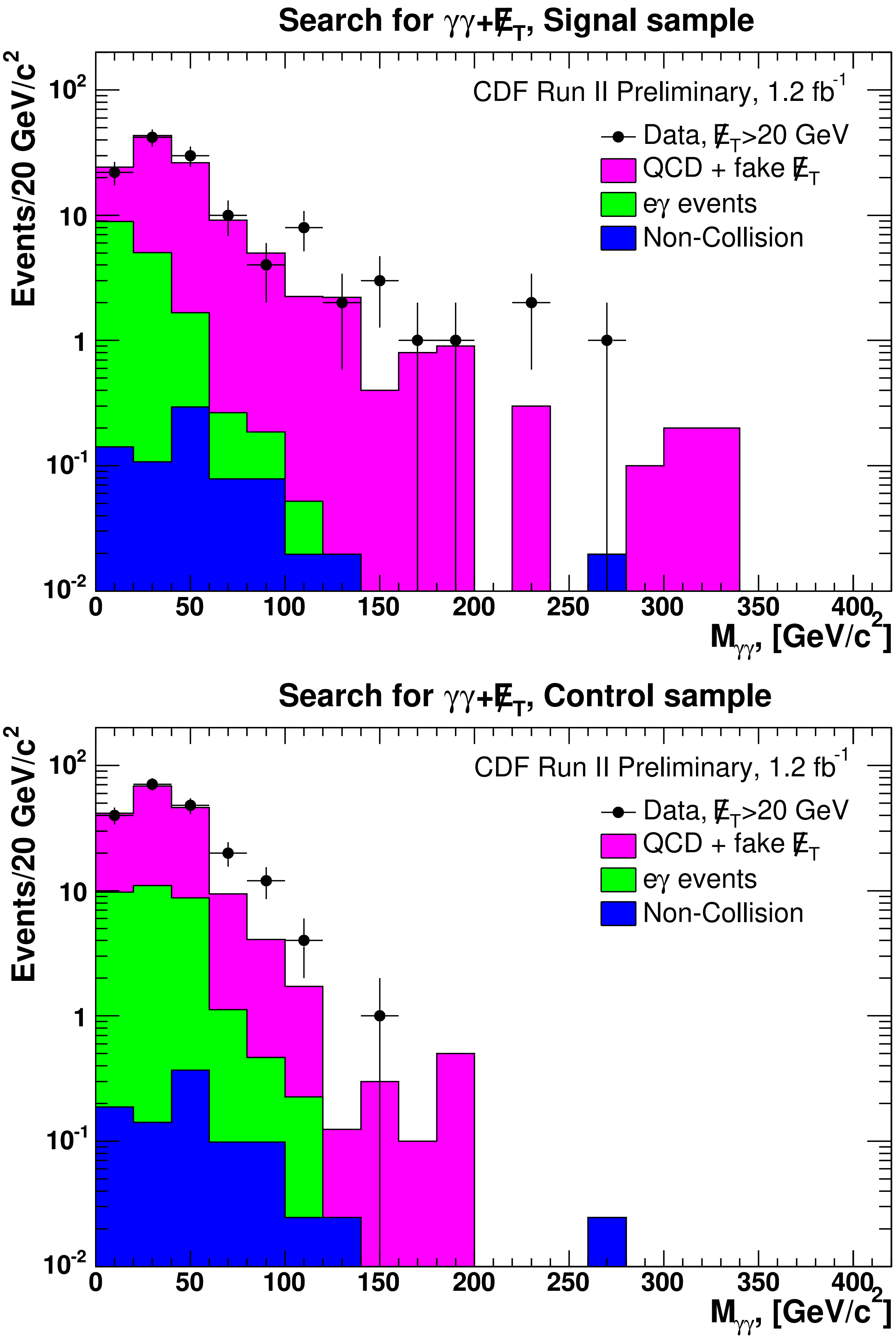

FIG. 3: The $M_{\gamma\gamma}$ distribution for $\gamma\gamma$ control (top) and signal (bottom) events with $\not{E}_t > 20$ GeV.

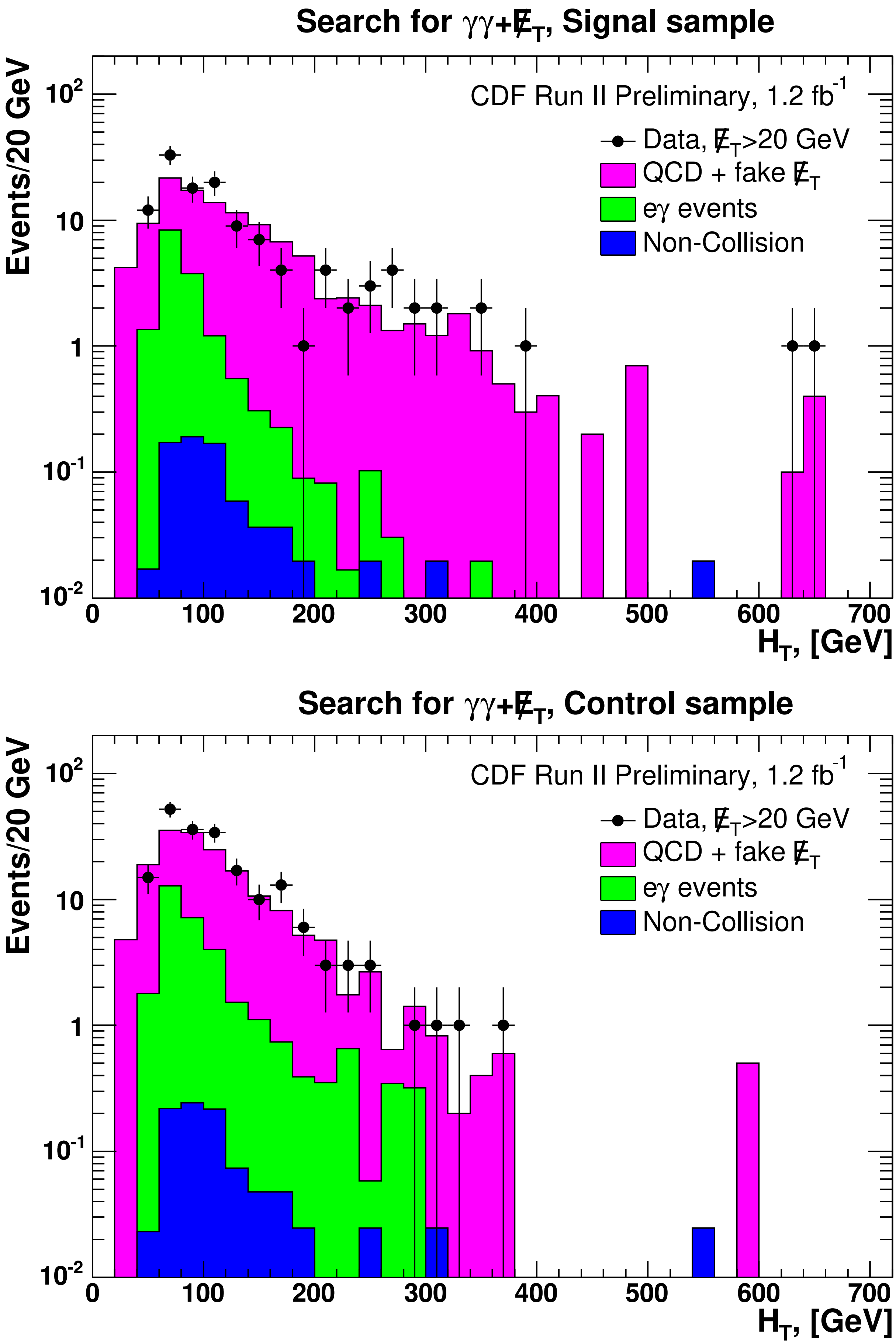

FIG. 4: The H_T distribution for $\gamma\gamma$ control (top) and signal (bottom) events with $\not{E}_t > 20$ GeV.

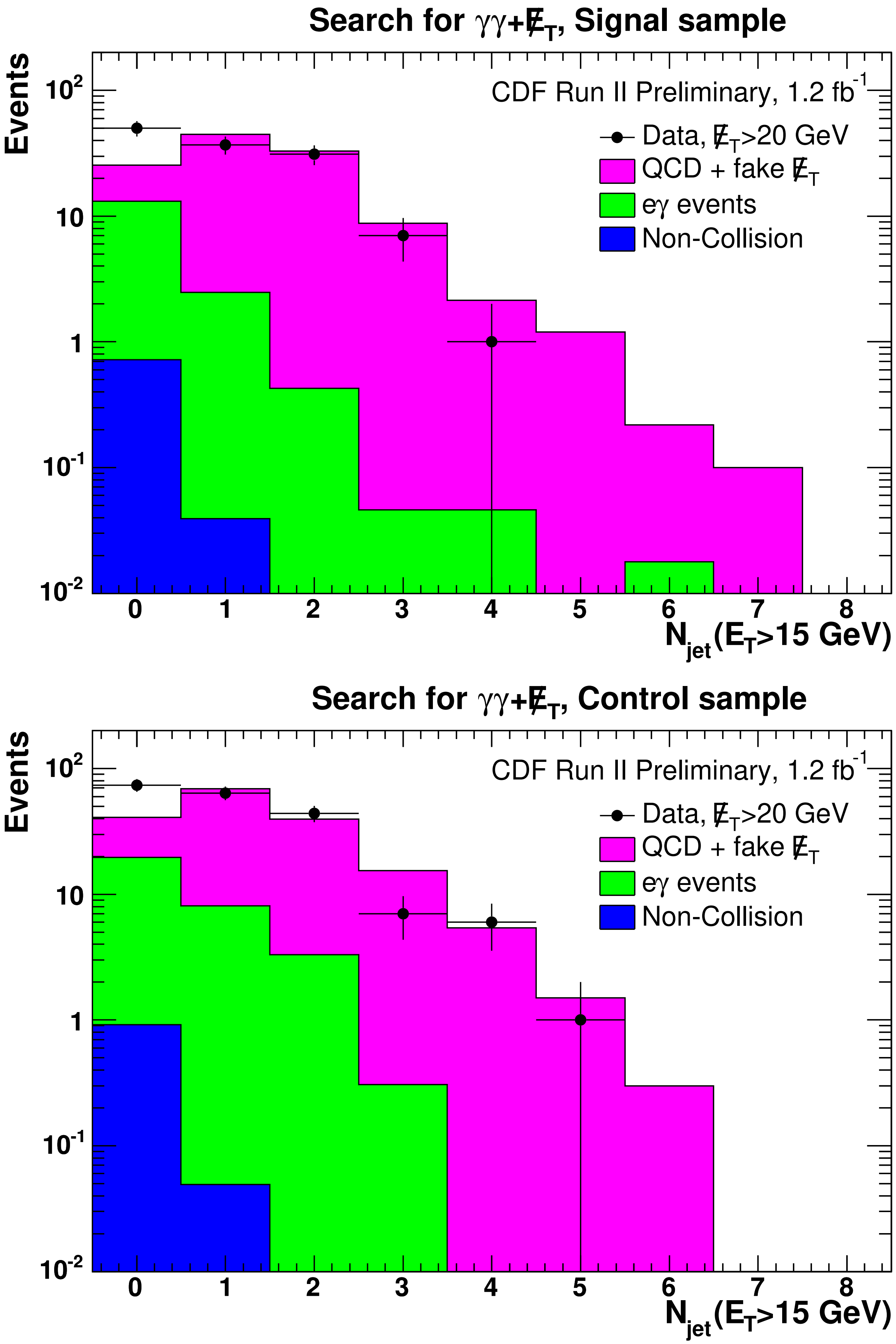

FIG. 5: The N_{jet15} distribution for $\gamma\gamma$ control (top) and signal (bottom) events with $\not\!E_t > 20$ GeV.

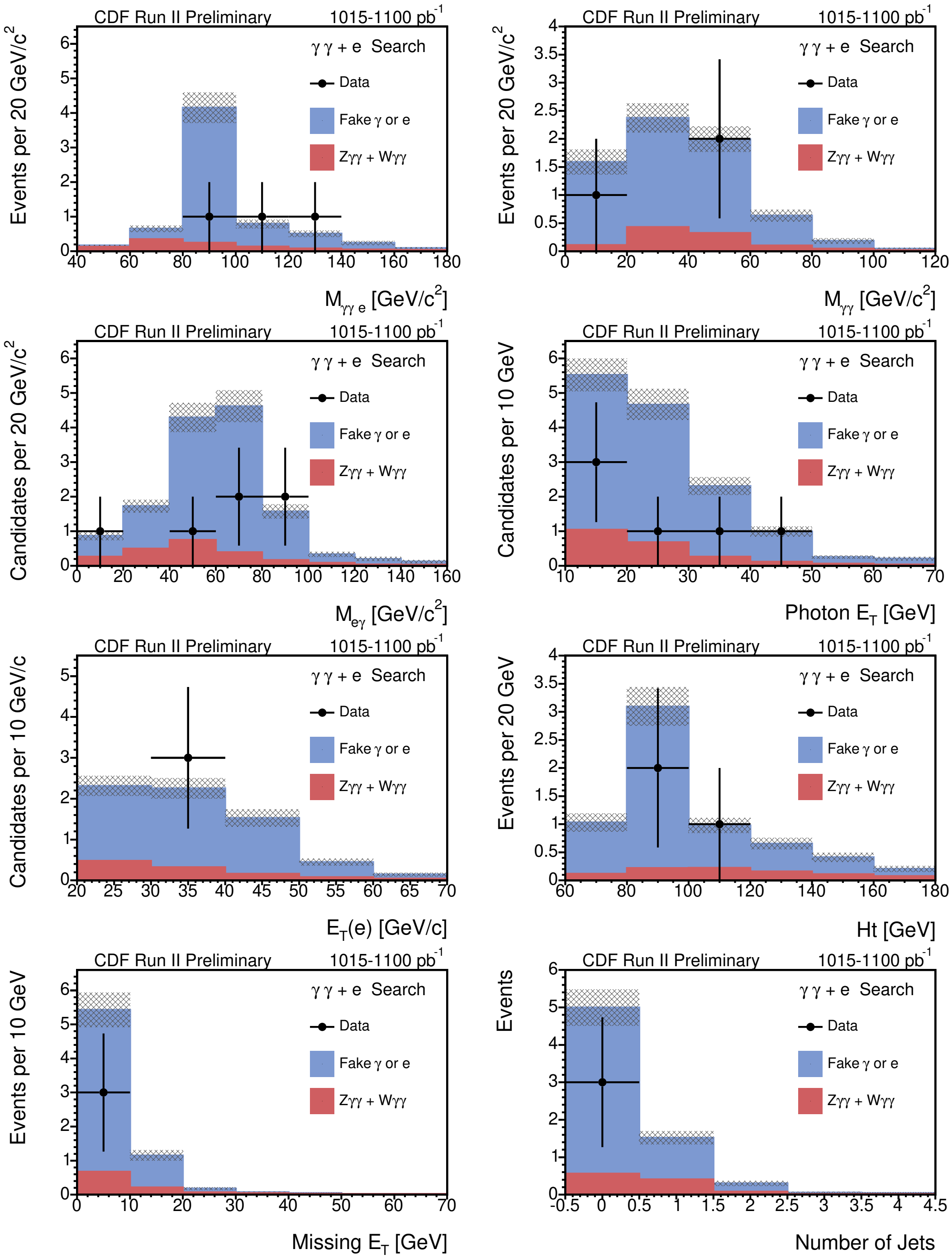

FIG. 6: Kinematic distributions of $\gamma\gamma e$ events from the SM (red filled histogram) + fake (blue filled histogram) prediction and those observed in the data (marker). Each photon is required to have an E_T greater than 13 GeV. Distributions from the top left to the bottom right are: three-body invariant mass, invariant mass of the diphoton, invariant mass of each electron-photon pair, E_T of each photon, E_T of the electron, H_T, missing E_T, and number of jets with a corrected E_T greater than 15 GeV in each event. Here, H_T refers to a sum E_T of all the identified objects (γ, e,μ, jet) and missing energy.

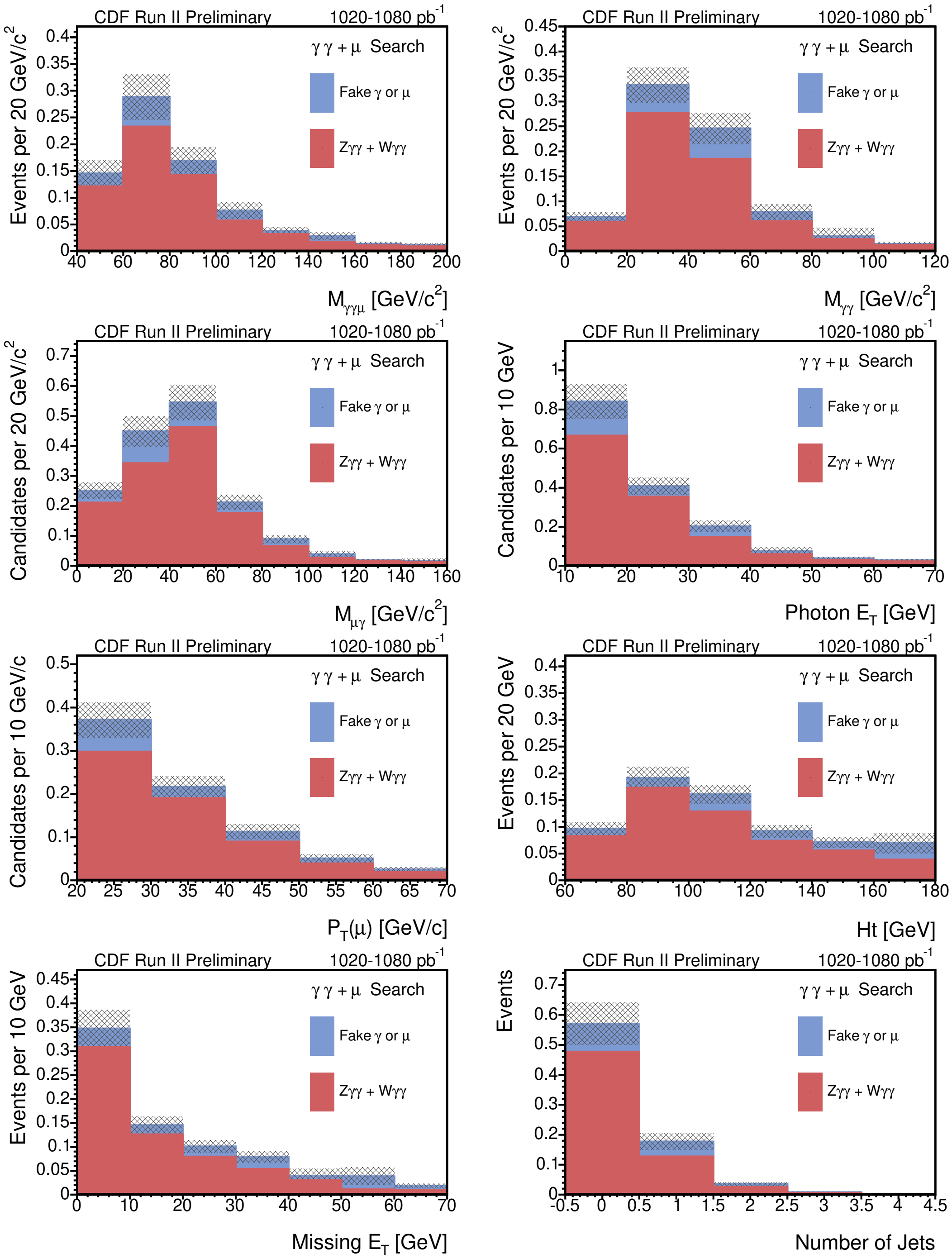

FIG. 7: Kinematic distributions of $\gamma\gamma\mu$ events from the SM (red filled histogram) + fake (blue filled histogram) prediction. We have observed zero event in data. Each photon is required to have an E_T greater than 13 GeV. Distributions from the top left to the bottom right are: three-body invariant mass, invariant mass of the diphoton, invariant mass of each muon-photon pair, E_T of each photon, P_T of the muon, H_T, missing E_T, and number of jets with a corrected E_T greater than 15 GeV in each event. Here, H_T refers to a sum E_T of all the identified objects (γ, e,μ, jet) and missing energy.

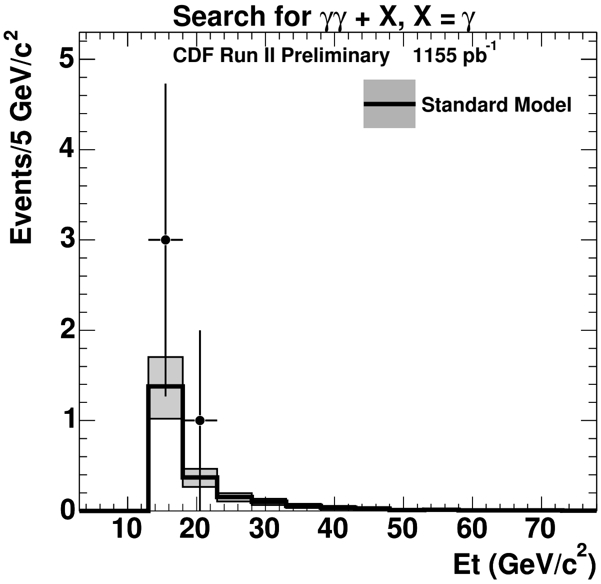

FIG. 8: The E_T for triphoton events.

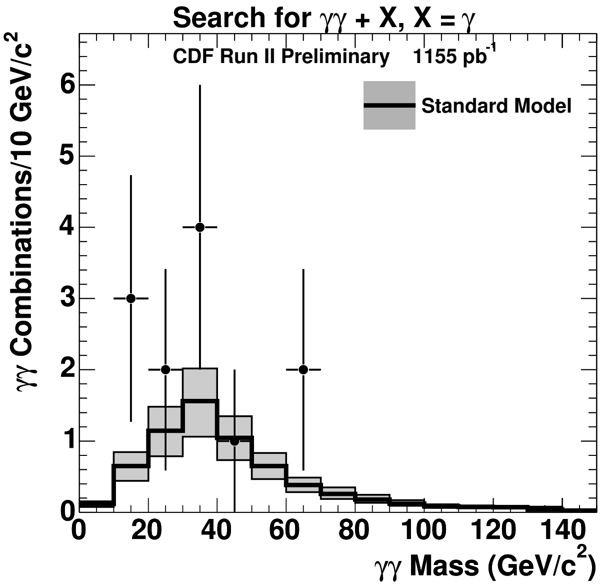

FIG. 9: The mass of all photon pairs for triphoton events.

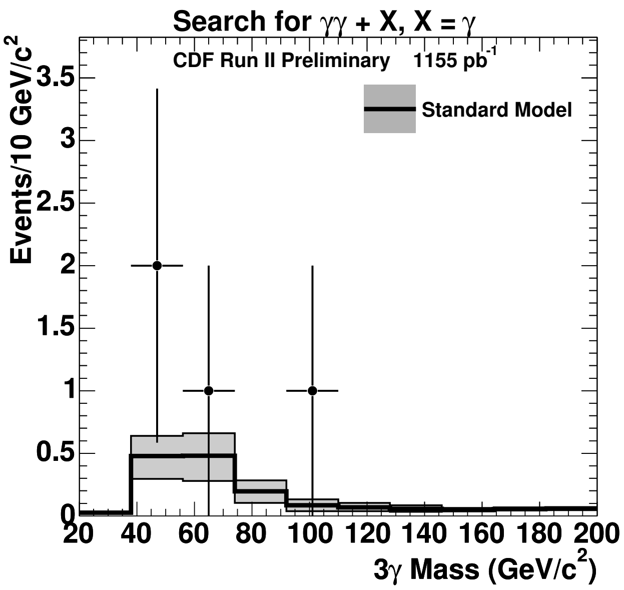

FIG. 10: The three-photon mass for triphoton events.

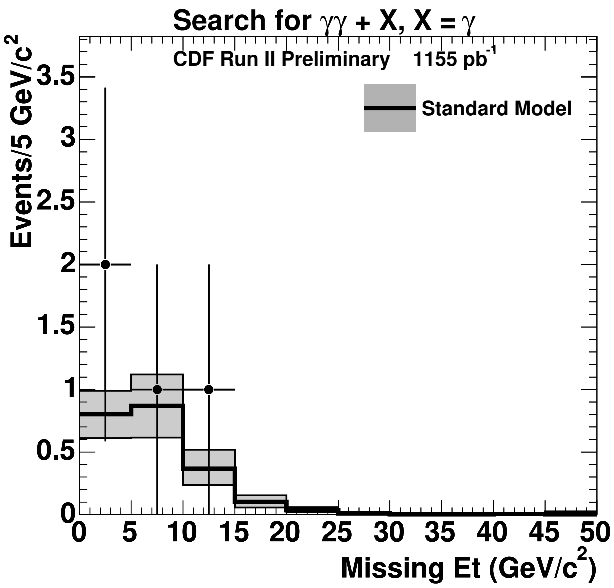

FIG. 11: The $\not\!\!E_t$for triphoton events.

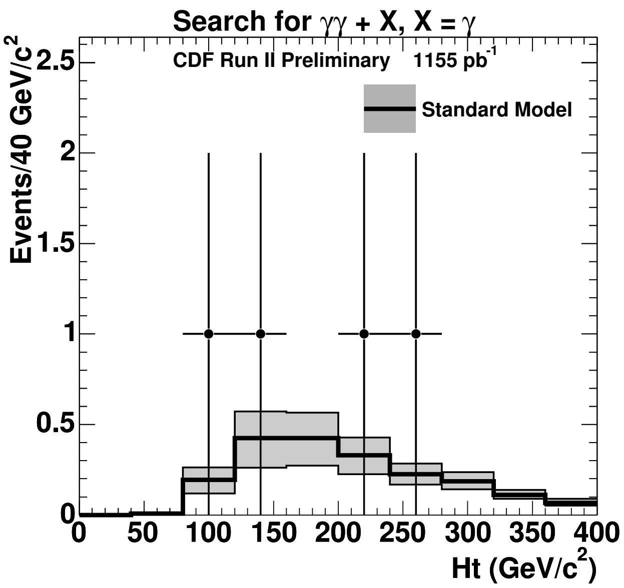

FIG. 12: The H_t for triphoton events. The H_t scalar sum includes the diphotons, the $\not{E}_t$, and jets with corrected $E_T > 15$ GeV.

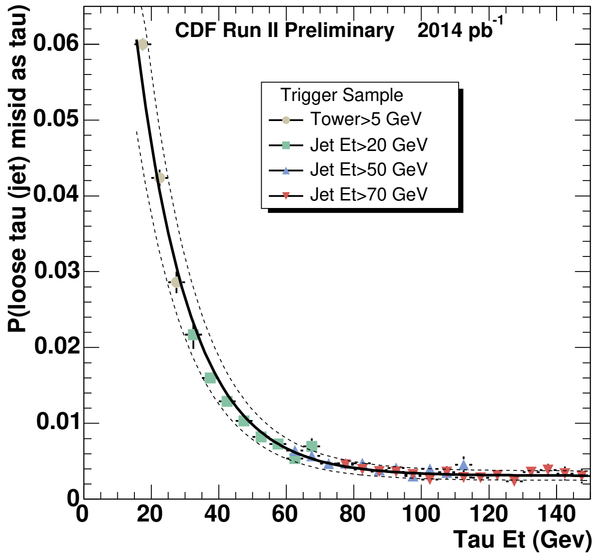

FIG. 13: The probablity that a loose tau from a jet fakes a tight tau.

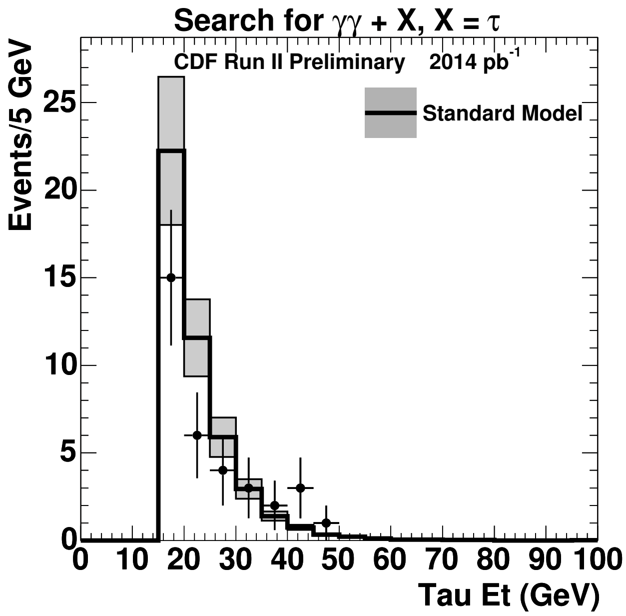

FIG. 14: The tau E_T for $\gamma\gamma\tau$ events.

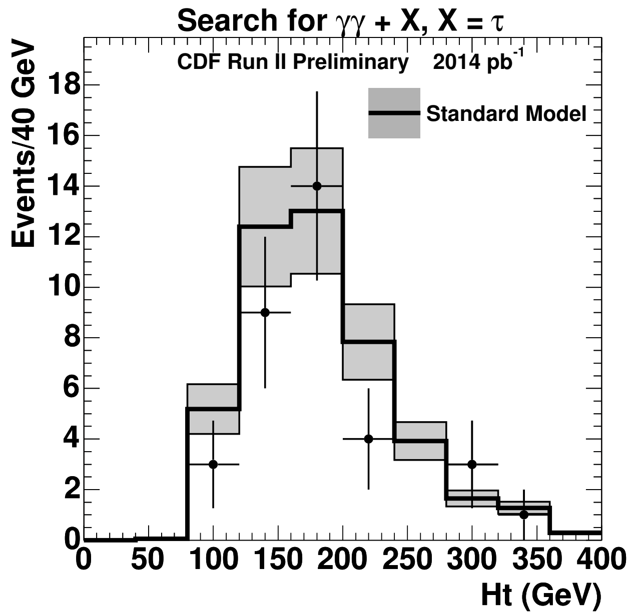

FIG. 15: The tau H_T for $\gamma\gamma\tau$ events.

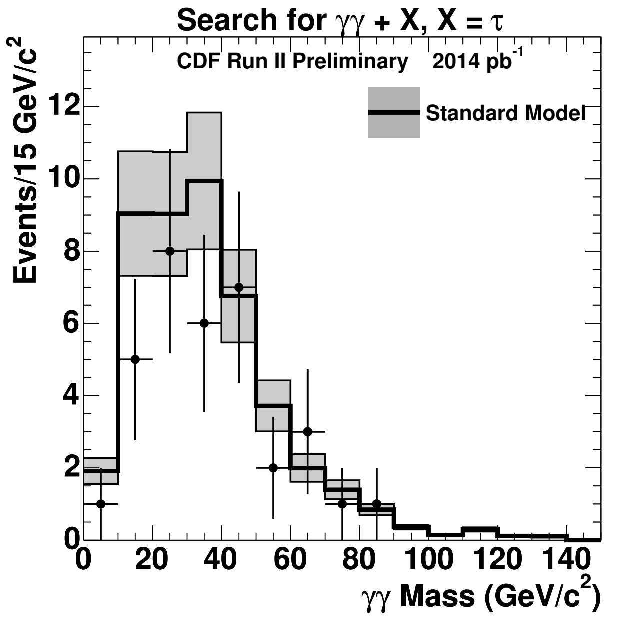

FIG. 16: The diphoton mass for $\gamma\gamma\tau$ events.

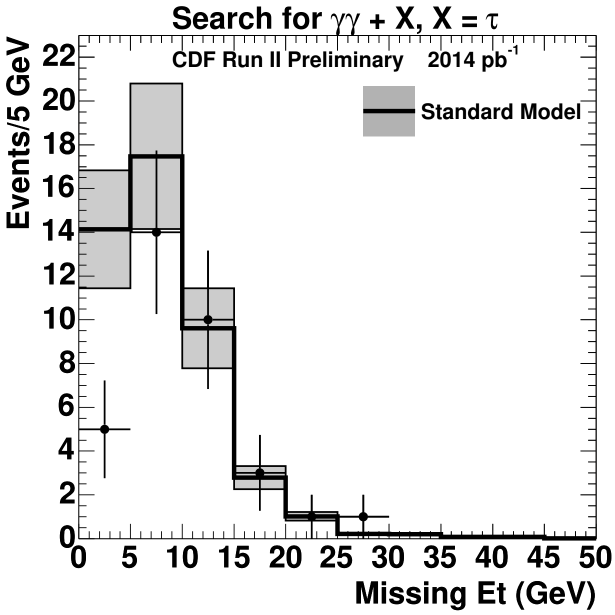

FIG. 17: The missing E_T for $\gamma\gamma\tau$ events.

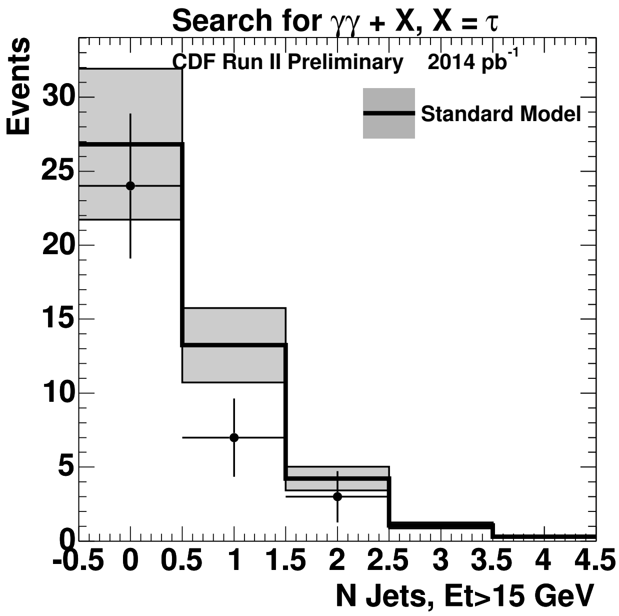

FIG. 18: The number of jets with corrected $E_T > 15$ GeV for $\gamma\gamma\tau$ events.